Eur. Phys. J. A **30**, 531–539 (2006)
DOI 10.1140/epja/i2006-10149-x

THE EUROPEAN PHYSICAL JOURNAL A

Microscopic study of yrast bands and backbending anomaly in $^{78-82}$Kr isotopes

S. Verma, R. Devi[a], and S.K. Khosa

Department of Physics and Electronics, University of Jammu, Jammu-180006, India

Received: 29 June 2006 / Revised: 24 November 2006 /
Published online: 18 December 2006 –
Communicated by R. Krücken

Abstract. The yrast spectra of $^{78-82}$Kr are studied by using the projected shell model (PSM) approach. The energy states are obtained by taking oblate as well as prolate quadrupole deformations for $^{78-82}$Kr. The structure of yrast states and backbending phenomena are investigated. The theoretical results predict low-lying states in ^{78,82}Kr to be oblate and coexistence of oblate-prolate shapes for ^{80}Kr. The $B(E2)$ transition probabilities and g-factors are obtained and compared with the available experimental data.

PACS. 21.60.Cs Shell model – 21.10.Ky Electromagnetic moments – 21.10.Re Collective levels – 27.50.+e
$59 \leq A \leq 89$

1 Introduction

The study of high-spin states in many Kr isotopes has attracted a considerable interest in recent years. A rich variety of shapes, as well as shape coexistence, have been seen in the $^{78-82}$Kr isotopes [1–14]. The available data on $^{78-82}$Kr isotopes [5–7,9,10,14] provide some interesting observations at high spin. Some time back, the yrast band of ^{78}Kr has been extended to higher spins up to $26\hbar$ by Joshi *et al.* [6] and Sun *et al.* [5]. Recently, Dhal *et al.* [7] have measured the lifetimes in ^{78}Kr up to the $I^{\pi} = 22^{+}$ level by using the Doppler shift attenuation method. The transition quadrupole moments deduced from the lifetimes show a decreasing trend with the rotational frequency. In the case of ^{80}Kr, the previously known positive-parity yrast band has been extended to a high spin of 20^{+} by Doring *et al.* [9]. Mukherjee *et al.* [10] have measured the lifetimes of the yrast band of ^{80}Kr and deduced the transition quadrupole moments ($Q_{\rm t}$) that show a decreasing tendency after the band crossing. Thus, the decreasing trend of $Q_{\rm t}$ indicates a change in shape at high spin in this band. Kemnitz *et al.* [1] have identified the excited states in ^{82}Kr up to $I = 12\hbar$ by using in-beam γ-ray spectroscopy. Recently, Mertzimekis *et al.* [14] for the first time measured g-factors of the 2_1^+ and 4_1^+ states in $^{78-82}$Kr, using the Coulomb excitation of isotopic Kr beams and the transient-field technique.

In the past some theoretical attempts have been made to study the high-spin states and to investigate the shape coexistence phenomenon in even-even Kr isotopes. These theoretical investigations come to different conclusions concerning the oblate and prolate nature of different calculated bands as well as the proton and neutron alignment. The nucleus ^{78}Kr has been studied extensively by using different theoretical models. Gross *et al.* [3] used the cranked shell model and shell correction method with the Woods-Saxon average field and pairing term. They concluded that the first backbending in the ^{78}Kr yrast line is due to the alignment of a pair of $g_{9/2}$ protons, while the second irregularity is interpreted in terms of the $g_{9/2}$ neutron alignment inducing a shape change from $\gamma \approx 15^{\circ}$ to $\gamma = -30^{\circ}$. Billowes *et al.* [4] supported the assignment of the $g_{9/2}$ neutron alignment at the first band crossing by measuring average g-factors in ^{78}Kr. Tripathy and Sahu [15] studied the structure of the collective bands in ^{78}Kr within the framework of the deformed configuration mixing shell model based on Hartree-Fock states and found that the prolate-deformed ground-state band crosses at 8^{+} a neutron-aligned band which becomes yrast. Recently, Jakhar *et al.* [16] have studied the yrast band of ^{78}Kr by using fully the self-consistent cranked-Hartree-Fock-Bogoluibov approach with a pairing plus quadrupole plus hexadecapole model interaction Hamiltonian. They conclude that the shape of ^{78}Kr remains prolate all through up to $I = 24$.

An extensive analysis of quasiparticle excitations around mass $A \approx 80$ has been presented in ref. [17] and two-quasiparticle-plus-rotor calculations at prolate deformation have been performed by Sastry *et al.* [8]. In both papers the conclusion was drawn that in ^{80}Kr at spins $8\hbar$ and $10\hbar$, the positive-parity ground-state band is crossed by an aligned two-quasiparticle $g_{9/2}$ proton band. Doring

[a] e-mail: rani_rakwal@yahoo.co.in

et al. [9] have studied the band structure of ^{80}Kr. The level scheme shows that the ground-state positive-parity band is crossed by a two-quasiproton (2qp) band at a rotational frequency $\hbar\omega \sim 0.5\,\mathrm{MeV}$ and becomes yrast above the 8^+ state. They performed total Routhian surface (TRS) and cranked shell model (CSM) calculations for ^{80}Kr. The TRS calculations predicted an oblate shape with $\beta_2 = 0.25$. The CSM calculations performed for an oblate shape with $\beta_2 \sim 0.25$ predict a two-quasineutron alignment at $\hbar\omega \approx 0.50\,\mathrm{MeV}$ and a two-quasiproton alignment at $\hbar\omega = 0.72\,\mathrm{MeV}$. Moreover, the observed gain in the aligned angular momentum, $\sim 6\hbar$ at $\hbar\omega \approx 0.50\,\mathrm{MeV}$, indicates a simultaneous alignment of two quasineutrons and two quasiprotons. Mukherjee *et al.* [10] have performed Hartree-Fock-Bogoluibov cranking model calculations with the Woods-Saxon potential and monopole pairing to understand the shape and particle alignments in the yrast band of ^{80}Kr at high spin. The TRS calculations performed within this model suggest that the change in the quadrupole moment is due to the change in shape in ^{80}Kr from near oblate to near prolate with lower deformation at high spin. The large gain in aligned angular momentum is due to the simultaneous alignment of neutron and proton pairs. The results of IBM calculations performed by Dejbakhsh *et al.* [18] for $^{78-82}$Kr show reasonable agreement with the experimental data. The systematics of the first 2^+ state g-factors in the mass-80 region were investigated by Mertzimekis *et al.* [19] in terms of an IBM-II analysis, a pairing-corrected geometrical model and a shell model approach. The nuclei in the mass-80 region show transitional structures and a complex interplay of single-particle and collective features.

In the present work we have performed projected shell model (PSM) calculations for both prolate as well as oblate deformations for $^{78-82}$Kr isotopes. In sect. 2, the outline of PSM is presented. In sect. 3, the yrast spectra obtained by PSM calculations are compared with the experimental data. To check the reliability of the PSM wave functions, the $B(E2)$ transition probabilities and g-factors are calculated and compared with the experimental data in sect. 3. Finally, in sect. 4 some conclusions are drawn.

2 Projected shell model

For a detailed theory of the PSM, the reader is referred to the review article [20]. Here, we present an outline of the model. For the present study, we include 0-, 2- and 4-quasiparticle (qp) states $|\Phi_\kappa\rangle$ as

$$\big\{|0\rangle, \alpha^\dagger_{\nu_i}\alpha^\dagger_{\nu_j}|0\rangle, \alpha^\dagger_{\pi_m}\alpha^\dagger_{\pi_n}|0\rangle, \alpha^\dagger_{\nu_i}\alpha^\dagger_{\nu_j}\alpha^\dagger_{\pi_m}\alpha^\dagger_{\pi_n}|0\rangle\big\}, \quad (1)$$

for doubly even nuclei, where $a^\dagger$ is the creation operator for a single quasiparticle and the index $\nu(\pi)$ denotes neutrons (protons). The many-body wave function is a superposition of projected (angular momentum) multi-quasiparticle states,

$$\big|\Psi^I_M\big\rangle = \sum_{\kappa K} f^I_{\kappa K} P^I_{MK}|\phi_\kappa\rangle, \quad (2)$$

where P^I_{MK} are the angular-momentum projection operators. The coefficients $f^I_{\kappa K}$ are the weights of the basis state κ and are determined by the diagonalization of the shell model Hamiltonian in the space spanned by the projected basis states given above. The PSM eigenvalue equation is given by

$$\sum_\kappa \big(H^I_{\kappa K} - E N^I_{\kappa K}\big) f^I_{\kappa K} = 0,$$

where the Hamiltonian and norm matrix elements are defined by

$$H^I_{\kappa K} = \langle\phi_\kappa|\hat{H}\hat{P}^I_{M_\kappa N_K}|\phi_K\rangle$$

and

$$N^I_{\kappa K} = \langle\phi_\kappa|\hat{P}^I_{M_\kappa N_K}|\phi_K\rangle.$$

The projection of an intrinsic state, $|\phi_\kappa\rangle$, onto a good angular momentum will generate the rotational energy as

$$E_\kappa(I) = \frac{\langle\phi_\kappa|\hat{H}\hat{P}^I_{KK}|\phi_\kappa\rangle}{\langle\phi_\kappa|\hat{P}^I_{KK}|\phi_\kappa\rangle} = \frac{H^I_{\kappa\kappa}}{N^I_{\kappa\kappa}}.$$

It represents the expectation value of the Hamiltonian with respect to a projected quasiparticle state κ. A diagram in which rotational energies of various bands are plotted against the spin I will be referred to as a band diagram which contains incredibly rich information.

The usual separable-force Hamiltonian [20]

$$H = \hat{H}_0 - \frac{\chi}{2}\sum_\mu \hat{Q}^+_\mu\hat{Q}_\mu - G_\mathrm{M}\hat{P}^+\hat{P} - G_\mathrm{Q}\sum_\mu \hat{P}^+_\mu\hat{P}_\mu \quad (3)$$

has been used successfully to explain the system of rotational spectra for a large number of nuclei. The first term is the spherical single-particle Hamiltonian

$$\hat{H}_0 = \sum_\alpha c^\dagger_\alpha E_\alpha c_\alpha\,, \quad (4)$$

where $c^\dagger_\alpha$, c_α are the single-particle creation and annihilation operators, respectively, and E_α is the single-particle energy given by

$$E_\alpha = \hbar\omega\big[N - 2\kappa\hat{l}\cdot\hat{s} - \kappa\mu\big(\hat{l}^2 - \langle\hat{l}\rangle^2\big)\big], \quad (5)$$

where ω is the harmonic-oscillator parameter which incorporates the principle of volume conservation for nuclei deformed from spherical shapes, s and l represent the intrinsic nucleon spins and orbital momenta in the stretched coordinate basis. The Nilsson parameters κ and μ are taken from the N-dependent values of ref. [21]. The remaining terms in eq. (3) are the residual quadrupole-quadrupole, the monopole pairing and the quadrupole pairing interactions, respectively. The strength χ of the quadrupole-quadrupole term can be obtained via self-consistent conditions with a given deformation parameter, β_2, so it is not a true parameter. The value of β_2 was set according to the experimental observation, if available, for each nucleus in our calculation. In our calculations we have taken three major shells $N = 2, 3$ and 4 both for neutron and protons. The size of the qp basis in the present case is

about 60. The operators appearing in eq. (3) are defined as [20]

$$\hat{Q}_\mu = \sum_{\alpha\beta} c^\dagger_\alpha Q_{\mu\alpha\beta} c_\beta \,,$$

$$Q_{\mu\alpha\alpha'} = \sqrt{\frac{4\pi}{5}}\delta_{NN'} \left\langle Njm \left| \left(\frac{r}{b}\right)^2 Y_{2\mu} \right| N'j'm' \right\rangle ,$$

$$\hat{P} = \frac{1}{2}\sum_{\alpha} c^\dagger_\alpha c_{\bar{\alpha}} \,,$$

$$\hat{P}^+_\mu = \frac{1}{2}\sum_{\alpha\beta} c^\dagger_\alpha Q_{\mu\alpha\beta} c^\dagger_{\bar{\beta}} \,.$$

The strength of the quadrupole-quadrupole force was adjusted such that the known (input) quadrupole deformation (β_2) is obtained as a result of the self-consistent mean-field calculation. The monopole and quadrupole pairing interactions are given by

$$G_{\rm M} = \left(G_1 - G_2\frac{N-Z}{A}\right)\frac{1}{A}\,({\rm MeV}), \tag{6}$$

$$G_{\rm Q} = \gamma G_{\rm M}\,({\rm MeV}), \tag{7}$$

where $G_{\rm M}$ is inversely proportional to the particle number A and contains two adjustable constants G_2 and G_1. Adjusting the parameters, β_2, G_2 and G_1 will change the energy gap for each shell and thus will affect the selection of the quasiparticle basis. Here in our calculations G_1 is taken as 20.25 for both neutrons and protons and G_2 as 16.20(0) for neutrons (protons). The strength of the quadrupole-quadrupole pairing force, $G_{\rm Q}$, is assumed to be proportional to $G_{\rm M}$. One may carefully adjust the ratio of $G_{\rm Q}/G_{\rm M}$ during the calculation to get the best experimental observation representation. In the present calculation, the ratio of $G_{\rm Q}/G_{\rm M}$ is fixed as 0.16 for ^{78}Kr and 0.20 for ^{80,82}Kr. These strengths are the same as employed in the previous PSM calculation for this mass region [22]. After diagonalizing the Hamiltonian in the quasiparticle basis, the lowest energy for each spin is used to compare with the experimental yrast energy. The resulting wave functions are usually used to compute the $B(E2)$ transition strengths and gyromagnetic (g-) factors [23].

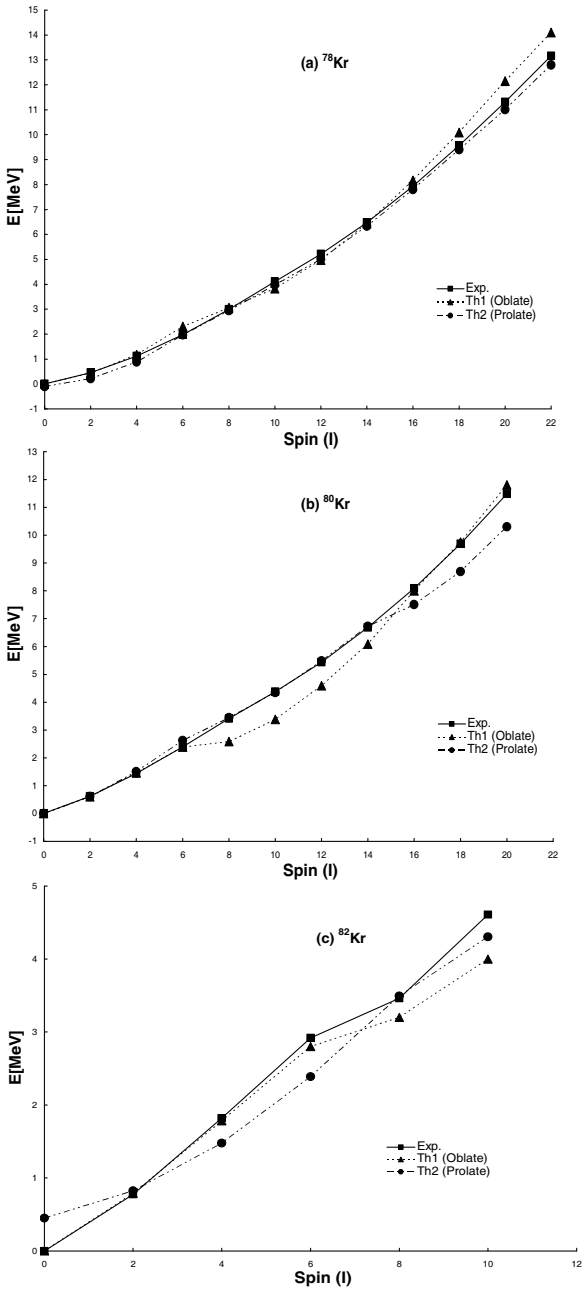

Fig. 1. Comparison of calculated yrast spectra with the experimental data for (a) ^{78}Kr, (b) ^{80}Kr and (c) ^{82}Kr.

3 Results and discussion

3.1 Yrast spectra

In figs. 1(a,b,c), the theoretical yrast spectra obtained by carrying out PSM calculations are compared with the experimental data for the $^{78-82}$Kr isotopes. In these figures, the yrast spectra obtained by carrying out PSM calculations for one oblate and one prolate deformation values are compared with the observed yrast spectra. Here the zero of the experimentally observed spectrum has been aligned with the zero of the oblate yrast spectrum. For the other prolate deformation, the yrast spectrum has been obtained relative to the above 0^+ reference energy. From the results presented in fig. 1(a), one observes that in the case of ^{78}Kr, the low-lying yrast spectrum up to $4\hbar$ is in better agreement with the yrast spectrum arising from an oblate minimum having quadrupole deformation $\beta_2 = -0.260$. The yrast states from 6^+ to 14^+ are found to be reproduced by energy states arising from the prolate as well as the oblate minimum. In the case of ^{80}Kr (fig. 1(b)), the low-lying yrast states up to 6^+ are seen to agree with the corresponding states arising from both oblate as well as prolate minima with $\beta_2 = -0.22$ and 0.207, respectively. The PSM calculations predict a coexistence of prolate and oblate shapes for the low-lying states. However, for states $8^+ \leq I \leq 14^+$, the energy states arising from the pro-

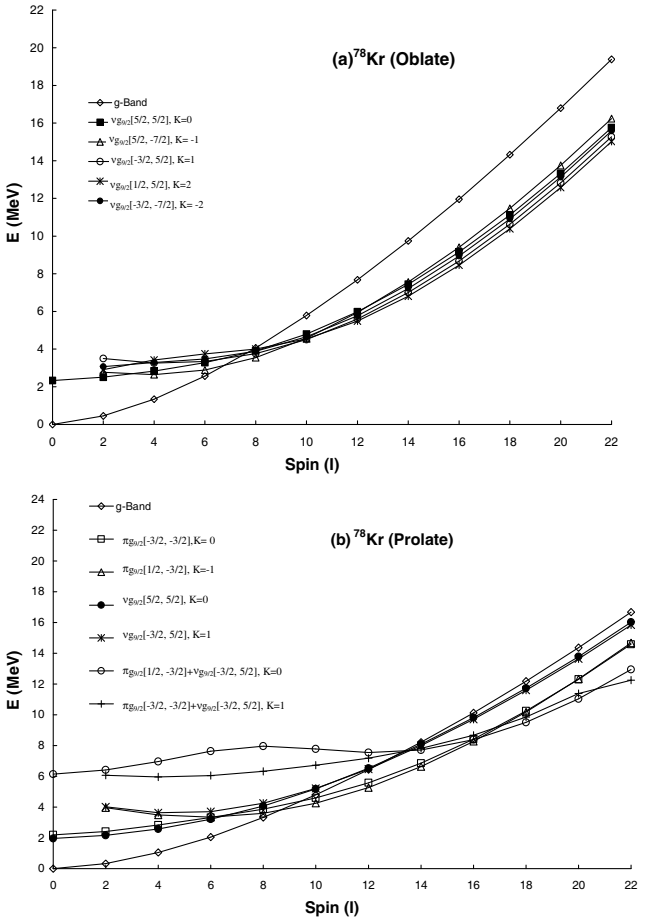

Fig. 2. Band diagrams (bands before configuration mixing) for ^{78}Kr at (a) the oblate minimum, and (b) the prolate minimum. Only the most important lowest-lying bands in each configuration are shown.

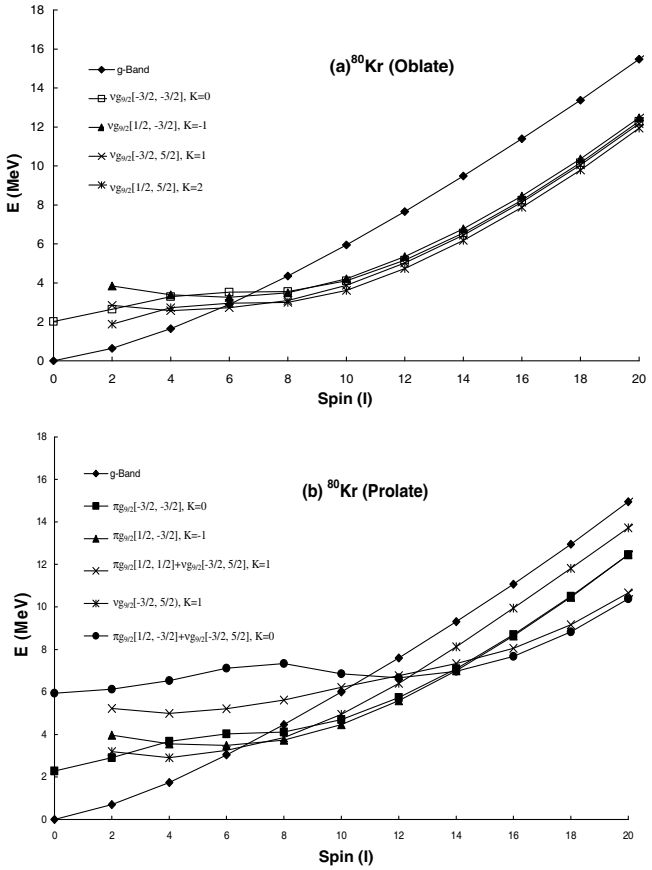

Fig. 3. Band diagrams (bands before configuration mixing) for ^{80}Kr at (a) the oblate minimum, and (b) the prolate minimum. Only the most important lowest-lying bands in each configuration are shown.

late minimum are in a reasonably better agreement than those arising from the oblate minimum. Further, it is noticed from this figure that yrast states with $I \geq 16^+$ show a better agreement with the corresponding states arising from the oblate minimum. In the case of ^{82}Kr (fig. 1(c)), the low-lying yrast states up to spin $4\hbar$ show a better agreement with the yrast spectra obtained from the oblate minimum. However, the higher states are seen to agree better with the yrast spectrum arising from the prolate deformation $\beta_2 = 0.202$.

We have also analysed the plots of yrast states *versus* spin by aligning the 0^+ state arising from the prolate deformation with the experimental 0^+ for $^{78-82}$Kr. The observations as pointed out earlier in this section undergo a marginal change. In the case of ^{80}Kr, it turns out that the low-lying states below 6^+ are equally well reproduced by oblate and prolate minima, whereas in ^{78,82}Kr the energy values arising from the oblate minimum for $2^+ \leq I \leq 6^+$ are in better agreement with the experiment than those arising from the prolate minimum.

From the above discussion one thing is clear that the prolate and oblate yrast solutions in $^{78-82}$Kr isotopes are reasonably close over all ranges of spin. It is true that the comparison with the experimental yrast spectra does not help very much to discriminate between different shapes for the low-lying yrast spectra but the type of agreement obtained is indicative of the fact that at least the low-lying states of the yrast spectra can be thought to be arising from a composite state $|\Psi^J\rangle$ which is a superposition of the projected states $|\Psi^J_{\rm o}\rangle$ from the oblate minimum and $|\Psi^J_{\rm p}\rangle$ from the prolate minimum, such that

$$\left|\Psi^J\right\rangle = a^J_{\rm o}\left|\Psi^J_{\rm o}\right\rangle + a^J_{\rm p}\left|\Psi^J_{\rm p}\right\rangle, \tag{8}$$

where the values of $a^J_{\rm o}$ and $a^J_{\rm p}$ give a measure of the extent of mixing of oblate and prolate shapes.

Normalization of the state $|\Psi^J\rangle$ gives the equation

$$\left|a^J_{\rm o}\right|^2 + \left|a^J_{\rm p}\right|^2 + a^{*J}_{\rm o} a^J_{\rm p}\left\langle\Psi^J_{\rm o} \mid \Psi^J_{\rm p}\right\rangle + a^J_{\rm o} a^{*J}_{\rm p}\left\langle\Psi^J_{\rm p} \mid \Psi^J_{\rm o}\right\rangle = 1. \tag{9}$$

In figs. 2, 3 and 4, the band diagrams for $^{78-82}$Kr have been displayed. For each band we have marked its quasiparticle configuration. In PSM calculations, we obtain 60 bands but in the figures only those bands are plotted that cross the ground-state band and whose weight factors are ≥ 0.10. From the band diagrams obtained for oblate solutions, it is observed that the low-lying states from 0^+ to 6^+ in ^{78}Kr, 0^+ to 4^+ in ^{80}Kr and 0^+ to 4^+ in ^{82}Kr are

Table 1. Theoretical mixing ratios $a_{\rm o}^J$, $a_{\rm p}^J$ and transition quadrupole moments $q_{\rm o}^J$, $q_{\rm p}^J$ for oblate and prolate deformations for $^{78-82}$Kr. The seventh column presents the experimental transition quadrupole moments ($q_{\rm exp}^J$) for $^{78-82}$Kr. The experimental data for ($q_{\rm exp}^J$) for $^{78-80}$Kr is taken from refs. [6,10].

Nucleus	Low-lying states below first crossing	$a_{\rm o}^J$	$a_{\rm p}^J$	$q_{\rm o}^J$	$q_{\rm p}^J$	$q_{\rm exp}^J$	$e_{\rm eff}$
^{78}Kr	2_1^+	0.891	0.108	2.49	3.045	2.55	0.7
	4_1^+	0.984	0.015	2.500	3.110	2.51	0.7
	6_1^+	0.969	0.030	2.406	3.188	2.43	0.7
^{80}Kr	2_1^+	0.5	0.5	1.975	1.974	1.95	0.585
	4_1^+	0.5	0.5	2.111	1.993	1.84	0.585
^{82}Kr	2_1^+	0.768	0.232	1.407	1.751	1.48	0.5
	4_1^+	0.768	0.232	1.512	1.773	1.57	0.5

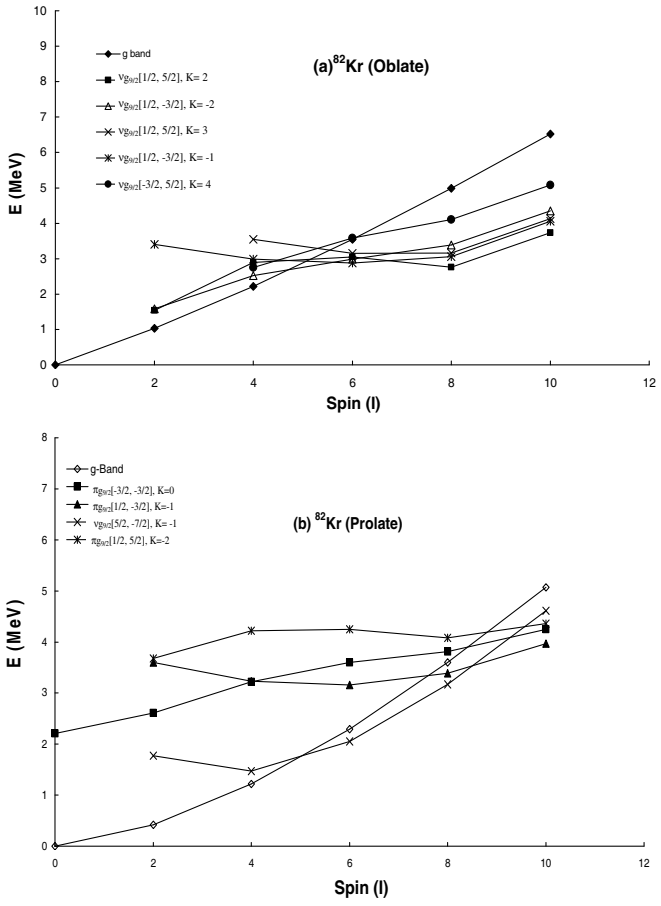

Fig. 4. Band diagrams (bands before configuration mixing) for ^{82}Kr at (a) the oblate minimum, and (b) the prolate minimum. Only the most important lowest-lying bands in each configuration are shown.

seen to arise from the 0-qp band whereas from the band diagrams arising from prolate solutions, one observes that the low-lying states from 0^+ to 8^+ in ^{78}Kr, 0^+ to 6^+ in ^{80}Kr and 0^+ to 4^+ in ^{82}Kr are seen to arise from the 0-qp band. In order to give quantitative estimates for $a_{\rm o}^J$ and $a_{\rm p}^J$, we have projected out the wave functions of the angular-momentum states below the first crossing in the band diagrams, separately for the states arising from the oblate and prolate minimum and calculated the transition quadrupole moments $q_{\rm o}^J$ and $q_{\rm p}^J$ for the nuclei $^{78-82}$Kr. We have then calculated the values of $a_{\rm o}^J$ and $a_{\rm p}^J$ by adopting the same procedure used for determining the mixing coefficients of s and d states in the case of deuteron by using the experimentally available transition quadrupole moments ($q_{\rm exp}^J$) for the various available low-lying angular-momentum states below the first crossing in $^{78-82}$Kr isotopes. Here

$$\langle\Psi|\hat{q}|\Psi\rangle = \left|a_{\rm o}^J\right|^2 q_{\rm o}^J + \left|a_{\rm p}^J\right|^2 q_{\rm p}^J + a_{\rm o}^{*J} a_{\rm p}^J q_{\rm p}^J \langle\Psi_{\rm o}^J \mid \Psi_{\rm p}^J\rangle + a_{\rm p}^{*J} a_{\rm o}^J q_{\rm o}^J \langle\Psi_{\rm p}^J \mid \Psi_{\rm o}^J\rangle = q_{\rm exp}^J\,. \quad (10)$$

It is found from the calculations that the value of the inner product of $|\Psi_{\rm p}^J\rangle$ and $|\Psi_{\rm o}^J\rangle$ is real and nearly equal to one. Equations (9) and (10) are simultaneously solved to obtain the real values of $a_{\rm o}^J$ and $a_{\rm p}^J$ in the range from zero to one.

In table 1, the values of $a_{\rm o}^J$, $a_{\rm p}^J$ $q_{\rm o}^J$, $q_{\rm p}^J$, $q_{\rm exp}^J$ and $e_{\rm eff}$ (where $e_{\rm eff}$ is the effective charge taken for each transition) are presented for $^{78-82}$Kr. From the results presented in this table, it is observed that in case of ^{78}Kr, the low-lying spectra up to 6^+ have more probability of arising from an oblate shape than from a prolate shape. The results indicate that the 6^+ state is nearly 96.9% oblate in ^{78}Kr. There are other works which support this inference. The configuration-dependent shell correction calculations [5] account nicely for the observed forking at high spins and predict an oblate shape at low to moderate spin, in agreement with the average g-factor measurement. Besides this, Galeriu *et al.* [24] predicted an oblate deformation of $\beta_2 = -0.32$ for ^{78}Kr and the calculations of Moller and Nix [25] also predicted an oblate ground-state deformation of $\beta_2 = -0.20$.

In case of ^{80}Kr there is equal probability for the low-lying states to arise from oblate and prolate deformations. The results are indicative of the coexistence of oblate and prolate shapes. The structure of the ^{80}Kr isotope is believed to be dominated at all spins by a strong oblate-

prolate competition with clear effects on the spectroscopic quadrupole moments as well as on the g-factors of the corresponding states. For ^{82}Kr the low-lying states have more probability of arising from an oblate shape. The results predict that 2^+ and 4^+ states in ^{82}Kr have 76.8% admixture of oblate wave function. Praharaj [26] has studied the low-lying positive-parity bands in ^{82}Kr by carrying out a deformed Hartree-Fock calculation with projection. This calculation shows that in ^{82}Kr there is sizable oblate-prolate shape mixing for the lowest 0^+ and 2^+ states, the oblate shape making the more dominant contribution. The energy spectrum obtained from angular-momentum projection and ortho-normalization in his calculation shows that the oblate shape makes a more dominant contribution.

3.2 Backbending phenomena

In figs. 5(a,b,c), the theoretical results of the moment of inertia $J^{(1)}$ *versus* the square of the rotational frequency (ω^2) are compared with the experimentally observed ones for $^{78-82}$Kr, respectively.

The kinematic moment of inertia $J^{(1)}$ is defined as

$$J^{(1)} = [(I - 1/2)/\omega] \quad (\hbar^2\,\mathrm{MeV}^{-1})$$

and the rotational frequency (ω) is defined as

$$\omega = [E(I) - E(I-2)]/2 \quad (\hbar\,\mathrm{MeV}).$$

Figure 2(a) represents the band diagram for ^{78}Kr, obtained by taking an oblate quadrupole deformation. It is evident from fig. 2(a) that in the spin range I = 6–10$\hbar$ the ground-state band is crossed by five 2-qp neutron bands having configurations $\nu g_{9/2}[5/2, 5/2]$, $K = 0$, $\nu g_{9/2}[5/2, -7/2]$, $K = -1$, $\nu g_{9/2}[-3/2, 5/2]$, $K = 1$, $\nu g_{9/2}[1/2, 5/2]$, $K = 2$ and $\nu g_{9/2}[-3/2, -7/2]$, $K = -2$. From the study of fig. 2(a), one is led to deduce that the occurrence of backbending in the yrast spectra arising from the oblate minimum may be attributed to the crossing of five 2-qp neutron bands around spin 8$\hbar$. Figure 2(b), represents the band diagram for ^{78}Kr, obtained by taking prolate quadrupole deformation. A look at this diagram shows that in the spin range I = 8–10$\hbar$, the ground-state band is crossed by two 2-qp proton bands having configurations $\pi g_{9/2}[1/2, -3/2]$, $K = -1$ and $\pi g_{9/2}[-3/2, -3/2]$, $K = 0$. A careful examination of the wave functions shows that these two 2-qp proton bands have weight factors twice the magnitude of that of five neutron bands in the case of oblate deformation. The occurrence of backbending in the prolate yrast spectra may be attributed to the crossing of the two proton 2-qp bands around spin 8$\hbar$. Above 14$\hbar$, the above two 2-qp bands are crossed by two 4-qp bands having configurations $\pi g_{9/2}[1/2, -3/2] + \nu g_{9/2}[-3/2, 5/2]$, $K = 0$ and $\pi g_{9/2}[-3/2, -3/2] + \nu g_{9/2}[-3/2, 5/2]$, $K = 1$ at spin 16$\hbar$.

From fig. 5(a), it may be noted that the experimentally observed backbending in ^{78}Kr around 10$\hbar$ is predicted to occur around 8$\hbar$ for the yrast spectra arising from oblate and prolate minima, respectively.

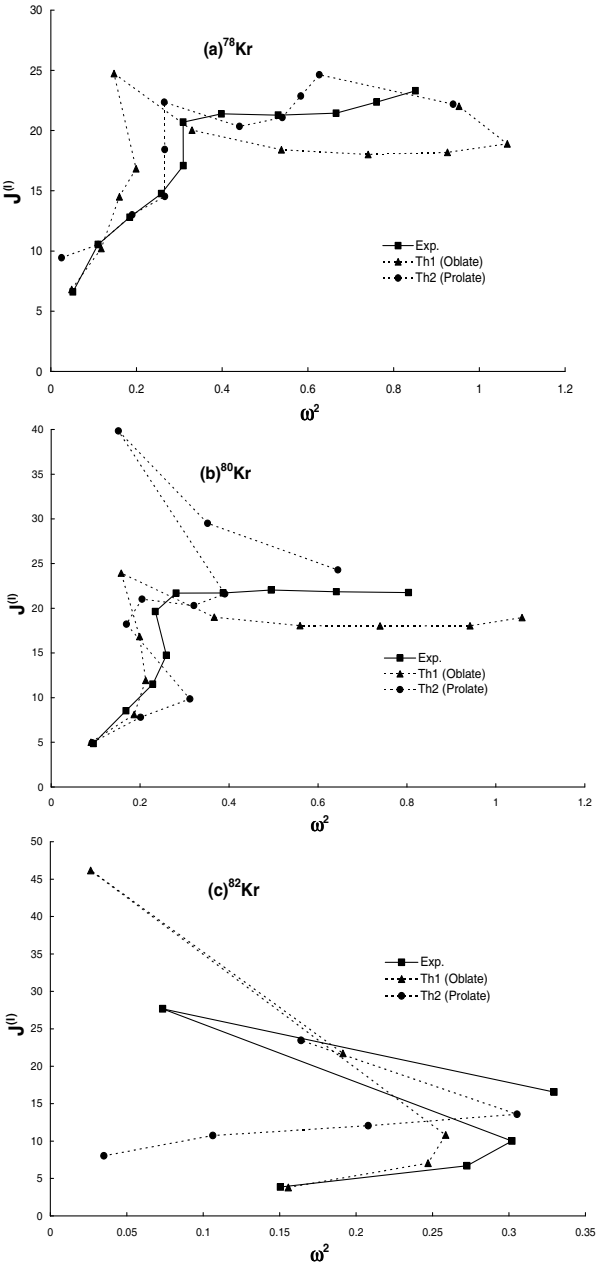

Fig. 5. Comparison of the calculated moment of inertia $J^{(1)}$ with the experimental one as a function of the square of the rotational frequency ω^2 for (a) ^{78}Kr, (b) ^{80}Kr and (c) ^{82}Kr.

In order to decide about the right mechanism responsible for the onset of backbending in ^{78}Kr, it is important to consider some additional piece of experimental information. An experimental determination of the small gyromagnetic factor for 8^+ in ref. [4] supports strongly an oblate yrast band and a crossing determined by $g_{9/2}$ neutron alignment. This measurement is actually considered as a proof of such a backbending [6,9,10]. In table 2, we present the values of g-factors for the states 2^+ to 8^+ for the oblate and prolate solutions for $^{78-82}$Kr isotopes. The

Table 2. Experimental (Exp.) and calculated (Th.) g-factors from 2_1 to 8_1 states in $^{78-82}$Kr (data taken from ref. [14]).

Nucleus	g-factors	Exp.	Th.	
			Oblate	Prolate
^{78}Kr	$g(2_1)$	+0.43(2)	+0.390	+0.312
	$g(4_1)$	+0.46(7)	+0.389	+0.376
	$g(6_1)$		+0.294	+0.440
	$g(8_1)$		−0.122	+0.556
^{80}Kr	$g(2_1)$	+0.38(5)	+0.257	+0.125
	$g(4_1)$	+0.46(15)	+0.228	+0.165
	$g(6_1)$		−0.132	+0.155
	$g(8_1)$		−0.221	−0.207
^{82}Kr	$g(2_1)$	+0.40(2)	+0.057	−0.023
	$g(4_1)$	+0.29(20)	+0.075	−0.037
	$g(6_1)$		−0.264	−0.027
	$g(8_1)$		−0.221	+0.136

g-factors $g(I)$, $g_\pi(I)$ and $g_\nu(I)$ are defined by [23]

$$g(I) = \frac{\mu(I)}{\mu_N I} = g_\pi(I) + g_\nu(I), \tag{11}$$

with

$$g_\tau(I) = \frac{1}{\mu_N [I(I+1)]^{1/2}} \times \left[g_l^\tau \langle \Psi_I \| \hat{J}^\tau \| \Psi_I \rangle + \left(g_s^\tau - g_l^\tau \right) \langle \Psi_I \| \hat{S}^\tau \| \Psi_I \rangle \right] \tag{12}$$

and $\mu(I)$ is the magnetic moment of a state (I).

In our calculations, the following standard values of g_l and g_s have been taken as $g_l^\pi = 1$, $g_l^\nu = 0$, $g_s^\pi = 5.586 \times 0.75$ and $g_s^\nu = -3.826 \times 0.75$. It can be seen from table 2 that the experimental values of $g(2_1)$ and $g(4_1)$ states for ^{78}Kr are reproduced by PSM calculations by taking an oblate minimum. It is important to note that the calculated value of $g(8^+)$ for ^{78}Kr arising from the oblate solution is 31% of the calculated value of $g(2^+)$ oblate, which is in qualitative agreement with the experimental observation. The $g(8^+)$ for the prolate solution is found to increase, which is in contradiction with experimental observations. Thus, we are constrained to conclude that the observed backbending in ^{78}Kr arises due to the crossing of five 2 $\nu g_{9/2}$-qp bands.

The theoretical yrast spectra presented in fig. 1(b) for ^{80}Kr, shows that the low-lying yrast states up to spin 6^+ are seen to arise from oblate and prolate minima. The band diagram of fig. 3(a) shows the crossing of four neutron 2-qp bands around spin $6\hbar$ whereas the band diagram for the prolate quadrupole deformation, fig. 3(b), shows that the ground-state band is crossed by two 2-qp proton bands and one 2-qp neutron band. The backbending plots obtained for the yrast energies arising from the prolate and oblate minima predict the occurrence of backbending at 6^+ whereas experimentally its onset takes place at $8\hbar$. The backbending occurring in the prolate yrast spectra may be attributed to the crossing of the ground-state band by two 2-qp prolate bands having configurations $\pi g_{9/2}[1/2, -3/2]$, $K = -1$ and $\pi g_{9/2}[-3/2, -3/2]$, $K = 0$. The yrast spectra for prolate deformation also exhibits a sharp backbend at $14\hbar$ which is not observed experimentally. The oblate yrast spectra, however, shows only one backbending commencing at $6\hbar$ and the cause for its occurrence may be attributed to the crossing of four neutron $g_{9/2}$ bands having configurations $\nu g_{9/2}[-3/2, -3/2]$, $K = 0$, $\nu g_{9/2}[1/2, -3/2]$, $K = -1$, $\nu g_{9/2}[-3/2, 5/2]$, $K = 1$, and $\nu g_{9/2}[1/2, 5/2]$, $K = 2$.

In order to decide about the right mechanism responsible for the onset of backbending in ^{80}Kr, we present in table 2, the values of g-factors from 2_1 to 8_1 states for the oblate and prolate solutions. The g-factors of ^{80}Kr for 2_1 and 4_1 states obtained from the oblate solution are in reasonable agreement with the experimental data. It may be noted that the $g(6_1)$ and $g(8_1)$ values obtained for oblate and prolate solutions are comparable to the corresponding $g(2_1)$ values suggesting thereby the onset of backbending in ^{80}Kr as arising due to the simultaneous crossing of $g_{9/2}$ proton and neutron bands. This observation is also supported by Mukherjee *et al.* [10].

The band diagrams for ^{82}Kr are presented in figs. 4(a,b). The yrast spectra of ^{82}Kr presented in fig. 1(c) show agreement with the yrast spectra obtained from the oblate minimum for the low-lying 0^+ to 4^+ states. The weight factors of these states corresponding to an oblate quadrupole deformation are larger in magnitude than those of the corresponding prolate states. Figure 4(a) presents the band diagram corresponding to the oblate deformation. It can be seen from fig. 4(a) that the ground-state band is crossed by five 2-qp neutron bands around spin $6\hbar$. The band diagram corresponding to the prolate quadrupole deformation shows that the ground-state band is crossed by one 2-qp neutron band around spin $6\hbar$ having configuration $\nu g_{9/2}[5/2, -7/2]$, $K = -1$ and by one 2-qp proton band around spin $8\hbar$ having configuration $\pi g_{9/2}[1/2, -3/2]$, $K = -1$. The observed backbending around spin $6\hbar$ is reproduced by PSM results obtained from the oblate minimum. The g-factors of low-lying states in the case of ^{82}Kr are not reproduced in the present PSM calculations.

3.3 B(E2) transition probabilities

$B(E2)$ transition probabilities can give important information on the nuclear structure and provide stringent test of a particular model.

The matrix elements of a quadrupole operator $\hat{Q}_{LM}$ with respect to the (final) shell model wave functions can be evaluated by using the formula [20]

$$\langle \Psi_{I_f M_f} | \hat{Q}_{LM} | \Psi_{I_i M_i} \rangle = (I_i M_i, LM | I_f M_f) \langle \Psi_{I_f} \| \hat{Q}_L \| \Psi_{I_i} \rangle. \tag{13}$$

The reduced transition probabilities $B(EL)$ from the initial state I_i to the final state I_f are given by [23]

$$B(EL, I_i \to I_f) = \frac{e^2}{(2I_i + 1)} \left| \langle \psi_{I_f} \| \hat{Q}_L \| \psi_{I_i} \rangle \right|^2, \tag{14}$$

Table 3. Experimental (Exp.) and calculated (Th.) $B(E2)$ reduced transition probabilities (in units of e^2b^2). Columns 4, 5 and 6 present the theoretical values of $B(E2)$ transitions obtained for oblate, prolate and mixed deformations, respectively. The effective charge used is given in the last column. Experimental data for $B(E2)$'s are taken from ^{78}Kr (ref. [6]), ^{80}Kr (ref. [10]) and ^{82}Kr (ref. [13]).

Nucleus	Transition	$B(E2)$'s				
		Exp	Th.			
	$I_f^+ \to I_i^+$		Oblate	Prolate	Mixed	e_{eff}
^{78}Kr	$2_1 \to 0_1$	0.1297(5)	0.1233	0.1845	0.1294	0.7
	$4_1 \to 2_1$	$0.1791^{+0.0109}_{-0.0096}$	0.1777	0.2749	0.1787	0.7
	$6_1 \to 4_1$	$0.1848^{+0.0565}_{-0.0351}$	0.1812	0.3182	0.1848	0.7
	$8_1 \to 6_1$	$0.1661^{+0.0256}_{-0.0195}$	0.0228	0.3323		0.7
	$10_1 \to 8_1$	$0.1489^{+0.0275}_{-0.0200}$	0.1773	0.0606		0.7
	$12_1 \to 10_1$	$0.1588^{+0.0397}_{-0.0265}$	0.2000	0.2507		0.7
	$14_1 \to 12_1$	$0.2108^{+0.0703}_{-0.0422}$	0.2110	0.2555		0.7
	$16_1 \to 14_1$	$0.0616^{+0.0206}_{-0.0123}$	0.2158	0.1746		0.7
	$18_1 \to 16_1$	$0.0317^{+0.0382}_{-0.0111}$	0.2131	0.1817		0.7
	$20_1 \to 18_1$	$0.0357^{+0.0643}_{-0.0140}$	0.1611	0.2242		0.7
	$22_1 \to 20_1$	$0.0181^{+0.0768}_{-0.0081}$	0.1667	0.2209		0.7
^{80}Kr	$2_1 \to 0_1$	0.076(6)	0.0776	0.0775	0.0776	0.585
	$4_1 \to 2_1$	$0.096^{0.027}_{0.016}$	0.1129	0.1266	0.1198	0.585
	$6_1 \to 4_1$	$0.206^{0.065}_{0.055}$	0.0868	0.1354		0.585
	$8_1 \to 6_1$	$0.172^{0.033}_{0.029}$	0.0606	0.0000		0.585
	$10_1 \to 8_1$	$0.165^{0.032}_{0.026}$	0.1172	0.0014		0.585
	$12_1 \to 10_1$	$0.186^{0.041}_{0.024}$	0.1314	0.1281		0.585
	$14_1 \to 12_1$	$0.102^{0.163}_{0.022}$	0.1430	0.0584		0.585
	$16_1 \to 14_1$	$0.047^{0.030}_{0.012}$	0.1520	0.0912		0.585
	$18_1 \to 16_1$	$0.043^{0.029}_{0.012}$	0.1554	0.1170		0.585
	$20_1 \to 18_1$	> 0.0286	0.1450	0.1178		0.585
^{82}Kr	$2_1 \to 0_1$	0.044(2)	0.0402	0.0610	0.0440	0.5
	$4_1 \to 2_1$	0.065(24)	0.0629	0.0890	0.0700	0.5

where the reduced matrix element is given by

$$\begin{aligned}
&\langle \psi_{I_f} \| \hat{Q}_L \| \psi_{I_i} \rangle \\
&= \sum_{\kappa_i,\kappa_f} f^{I_i}_{\kappa_i} f^{I_f}_{\kappa_f} \sum_{M_i,M_f,M} (-)^{I_f - M_f} \begin{pmatrix} I_f & L & I_i \\ -M_f & M & M_i \end{pmatrix} \\
&\quad \times \langle \phi_{\kappa_f} | \hat{P}^{I_f}_{K_{\kappa_f} M_f} \hat{Q}_{LM} \hat{P}^{I_i}_{K_{\kappa_i} M_i} | \phi_{\kappa_i} \rangle \\
&= 2 \sum_{\kappa_i,\kappa_f} f^{I_i}_{\kappa_i} f^{I_f}_{\kappa_f} \sum_{M',M''} (-)^{I_f - K_{\kappa_f}} (2I_f+1)^{-1} \begin{pmatrix} I_f & L & I_i \\ -K_{\kappa_f} & M' & M'' \end{pmatrix} \\
&\quad \times \int \mathrm{d}\Omega D_{M'' K_{\kappa_i}}(\Omega) \langle \phi_{\kappa_f} | \hat{Q}_{LM'} \hat{R}(\Omega) | \phi_{\kappa_i} \rangle. \qquad (15)
\end{aligned}$$

In table 3, the results of $B(E2)$ transition probabilities from $I \to I-2$ states are presented for $^{78-82}$Kr isotopes. These values are calculated from the corresponding wave functions of the oblate and prolate states. The estimates with a single value of effective charge do not give satisfactory agreement with experiments for higher transitions. From table 3, it is observed that the theoretical values of $B(E2)$ transitions obtained for a single value of effective (e_{eff}) charge for each isotope arising from the oblate solution are in reasonable agreement with the experimental data for the lower transitions.

Generally, e_{eff} charges are chosen to take into consideration the core-polarization effects. For a nucleus e_{eff} is proportional to Z/A. Raman *et al.* [27] have taken $e_{\text{eff}} = \varepsilon Z/A$ (for neutrons only) where ε is the proportionality constant. By choosing the proportionality constant around 1.5, the values of e_{eff} works out to be 0.69, 0.67 and 0.64 for $^{78-82}$Kr, respectively. We have chosen the values 0.7, 0.585 and 0.5 for ^{78,80,82}Kr, respectively, which are in close proximity to the above values. For ^{78}Kr the $B(E2)$ transition probabilities up to the transition $14 \to 12$ are

reproduced satisfactorily by the oblate solutions. However, for higher transitions the agreement is poor. In the case of ^{80}Kr, $B(E2)$'s for the lower transitions only are reproduced.

4 Conclusions

From the projected shell model study of $^{78-82}$Kr the following conclusions can be drawn:

1. The PSM calculations with quadrupole-quadrupole interaction plus monopole and quadrupole pairing force are found to reproduce the yrast spectra of $^{78-82}$Kr.
2. The calculations predict $I \leq 4^+$ states in the yrast spectra of ^{78}Kr to have more of oblate nature. These states are predicted to be composite states with $a_{\rm o} = 0.891$ and $a_{\rm p} = 0.108$ for the 2^+ state.
3. The PSM calculations predict a coexistence of prolate and oblate shapes for the low-lying states in ^{80}Kr.
4. The observed backbendings in ^{78,80}Kr around spins $10\hbar$ and $8\hbar$ are reproduced around spins $8\hbar$ and $6\hbar$, respectively. The results indicate that the backbending in case of ^{78}Kr arises from the the crossing of five 2-qp neutron oblate bands, whereas in ^{80}Kr the backbending may arise from the crossing of both oblate and prolate $g_{9/2}$ 2-qp bands.
5. In case of ^{82}Kr, the observed backbending around $6\hbar$ is reproduced by PSM results arising from oblate deformation.
6. The reduced $B(E2)$ transition probabilities are found to show satisfactory agreement with the experimental data for the lower transitions.
7. The experimental values of $g(2_1)$ and $g(4_1)$ for ^{78,80}Kr are reproduced by PSM calculations. The PSM calculations extract $g(2_1)$ and $g(4_1)$ from the intrinsic state having oblate deformation.

The authors are most grateful to Prof. Y. Sun and Prof. J.A. Sheikh for their collaborations and most valuable discussions.

References

1. P. Kemnitz, P. Odeja, J. Doring, L. Funke, L.K. Kostov, H. Rotter, E. Will, G. Winter, Nucl. Phys. A **425**, 493 (1984).
2. G. Winter, F. Dubbers, J. Doring, L. Funke, P. Kemnitz, E. Will, D.S. Andreev, K.I. Erochina, I.Kh. Lemberg, A.A. Pasternak, L.A. Rassadin, I.N. Chugunov, J. Phys. G: Nucl. Phys. **11**, 277 (1985).
3. C.J. Gross, J. Heese, K.P. Lieb, S. Ulbig, W. Nazarewicz, C.J. Lister, B.J. Varley, J. Billowes, A.A. Chishti, J.H. Mcneill, W. Gelletely, Nucl. Phys. A **501**, 367 (1989).
4. J. Billowes, F. Cristancho, H. Grawe, C.J. Gross, J. Heese, A.W. Mountford, M. Weiszflog, Phys. Rev. C **47**, R917 (1993).
5. H. Sun, J. Doring, G.D. Joshi, R.A. Kaye, G.Z. Solomon, S.L. Tabor, M. Devlin, D.R. LaFosse, F. Lerma, D.G. Sarantites, C. Baktash, D. Rudoph, C.-H. Yu, I.Y. Lee, A.O. Macchiavelli, I. Birriel, J.X. Saladin, D.F. Winchell, V.Q. Wood, I. Ragnarsson, Phys. Rev. C **59**, 655 (1999).
6. P.K. Joshi, H.C. Jain, R. Palit, G. Mukherjee, S. Nagaraj, Nucl. Phys. A **700**, 59 (2002).
7. A. Dhal, R.K. Sinha, P. Agarwal, S. Kumar, Monika, B.B. Singh, R. Kumar, P. Bringel, A. Neusser, R. Kumar, K.S. Golda, R.P. Singh, S. Muralithar, N. Madhavan, J.J. Das, A. Shukla, P.K. Raina, K.S. Thind, A.K. Sinha, I.M. Govil, P.K. Joshi, R.K. Bhowmik, A.K. Jain, S.C. Pancholi, L. Chaturvedi, Eur. Phys. J. A **27**, 33 (2006).
8. D.L. Sastry, A. Ahmed, A.V. Ramayya, R.B. Piercey, H. Kawakami, R. Soundranayagam, J.H. Hamilton, C.F. Maguire, A.P.de. Lima, S. Ramavataram, Phys. Rev. C **23**, 2086 (1981).
9. J. Doring, V.A. Wood, J.W. Holcomb, G.D. Johns, T.D. Johnson, M.A. Riley, G.N. Sylan, P.C. Womble, S.L. Tabor, Phys. Rev. C **52**, 76 (1995).
10. G. Mukherjee, H.C. Jain, R. Palit, P.K. Joshi, S.D. Paul, S. Nagaraj, Phys. Rev. C **64**, 034316 (2001).
11. J. Keinonen, K.P. Lieb, H.P. Hellmeister, A. Bockisch, A. Emling, Nucl. Phys. A **376**, 246 (1982).
12. S. Brussermann, J. Keinonen, H.P. Hellmeister, K.P. Leib, Z. Phys. A **304**, 335 (1982).
13. H.W. Muller, Nucl. Data Sheets **50**, 1 (1987).
14. T.J. Mertzimekis, N. Benczer-Koller, J. Holden, G. Jakob, G. Kumbartzki, K.-H. Speidel, R. Ernst, A. Macchiavelli, M. McMahan, L. Phair, P. Maier-Komor, A. Pakou, S. Vincent, W. Korten, Phys. Rev. C **64**, 024314 (2001).
15. K.C. Tripathy, R. Sahu, Nucl. Phys. A **597**, 177 (1996).
16. U.R. Jakhar, H.L. Yadav, A. Ansari, Pramana J. Phys. **65**, 1041 (2005).
17. L. Funke, J. Doring, F. Dubbers, P. Kemnitz, E. Will, G. Winter, V.G. Kiptilij, M.F. Kudojarov, I.Kh. Lemberg, A.A. Pasternak, A.S. Mishin, L. Hildingsson, A. Johnson, Th. Lindblad, Nucl. Phys. A **355**, 228 (1981).
18. H. Dejbakhsh, A. Kolomeits, S. Shlomo, Phys. Rev. C **51**, 573 (1995).
19. T.J. Mertzimekis, A.E. Stuchbery, N. Benczer-Koller, M.J. Taylor, Phys. Rev. C **68**, 054304 (2003).
20. K. Hara, Y. Sun, Int. J. Mod. Phys. E **4**, 637 (1995).
21. T. Bengtsson, I. Ragnarsson, Nucl. Phys. A **436**, 14 (1985).
22. R. Palit, J.A. Sheikh, Y. Sun, H.C. Jain, Nucl. Phys. A **686**, 141 (2001).
23. Y. Sun, J.L. Egido, Nucl. Phys. A **580**, 1 (1994).
24. D. Galeriu, D. Bucurescu, M. Ivascu, J. Phys. G: Nucl. Phys. **12**, 329 (1986).
25. P. Moller, J.R. Nix, At. Data Nucl. Data Tables **26**, 165 (1981).
26. C.R. Praharaj, J. Phys. G: Nucl. Phys. **14**, 843 (1982).
27. S. Raman, J.A. Sheikh, K.H. Bhatt, Phys. Rev. C **52**, 1380 (1995).